The Plant Cell, Vol. 23: 2696–2707, July 2011, www.plantcell.org

A Novel Calcium Binding Site in the Slow Vacuolar Cation Channel TPC1 Senses Luminal Calcium Levels [W]

Beata Dadacz-Narloch,[a] Diana Beyhl,[a] Christina Larisch,[a] Enrique J. López-Sanjurjo,[a] Ralf Reski,[b] Kazuyuki Kuchitsu,[c] Thomas D. Müller,[a] Dirk Becker,[a] Gerald Schönknecht,[d,1] and Rainer Hedrich[a,e]

[a] University of Wuerzburg, Institute for Molecular Plant Physiology and Biophysics, D-97082 Wuerzburg, Germany
[b] Plant Biotechnology, Faculty of Biology, University of Freiburg, 79104 Freiburg, Germany
[c] Department of Applied Biological Science, Tokyo University of Science, Noda 278-8510 Japan
[d] Oklahoma State University, Department of Botany, Stillwater, Oklahoma 74078
[e] King Saud University, Riyadh 11451, Saudi Arabia

Cytosolic calcium homeostasis is pivotal for intracellular signaling and requires sensing of calcium concentrations in the cytosol and accessible stores. Numerous Ca^{2+} binding sites have been characterized in cytosolic proteins. However, little is known about Ca^{2+} binding inside organelles, like the vacuole. The slow vacuolar (SV) channel, encoded by *Arabidopsis thaliana TPC1*, is regulated by luminal Ca^{2+}. However, the D454/*fou2* mutation in TPC1 eliminates vacuolar calcium sensitivity and increases store calcium content. In a search for the luminal calcium binding site, structure modeling indicated a possible coordination site formed by residues Glu-450, Asp-454, Glu-456, and Glu-457 on the luminal side of TPC1. Each Glu residue was replaced by Gln, the modified genes were transiently expressed in loss-of-TPC1-function protoplasts, and SV channel responses to luminal calcium were recorded by patch clamp. SV channels lacking any of the four negatively charged residues appeared altered in calcium sensitivity of channel gating. Our results indicate that Glu-450 and Asp-454 are directly involved in Ca^{2+} binding, whereas Glu-456 and Glu-457 are probably involved in connecting the luminal Ca^{2+} binding site to the channel gate. This novel vacuolar calcium binding site represents a potential tool to address calcium storage in plants.

INTRODUCTION

As a versatile second messenger, cytosolic Ca^{2+} regulates numerous processes and binds countless targets (Hetherington and Brownlee, 2004; Dodd et al., 2010). A well-documented example is the rise in cytosolic calcium concentration in guard cells, which orchestrates the opening of diverse cation and anion channels in both the plasma membrane and vacuolar membrane, thereby accomplishing solute efflux and leading to stomatal closure (Schroeder et al., 2001; Dodd et al., 2010; Geiger et al., 2010). A lot less is known about changes in free calcium concentrations in organelles and how these changes might affect processes in storage sites such as the vacuole. The plant vacuole serves as a dynamic reservoir for various metabolites and ions. Among different cations, potassium, sodium, and calcium can accumulate in large quantities herein (Taiz, 1992; Bethmann et al., 1995). Potassium, as well as sodium content (under salt stress), can reach levels greater than 100 mM (Beyhl et al., 2009; Rienmüller et al., 2010), whereas luminal free calcium concentrations can get to 1 mM (Pottosin and Schönknecht, 2007). While the vacuolar Ca^{2+} concentration is more than 1000-fold higher compared with the cytosol, fluctuations of the extracytosolic Ca^{2+} concentration may exert biological actions, as has been demonstrated for extracellular calcium fluctuations (Han et al., 2003; Hofer, 2005).

The slow-activating vacuolar (SV) channel (Hedrich and Neher, 1987), encoded by *TPC1* in *Arabidopsis thaliana* (Peiter et al., 2005), is regulated by both cytosolic and luminal changes in Ca^{2+} concentration (Beyhl et al., 2009). The channel protein TPC1 harbors two cytosolic EF-hands for calcium binding, and rising cytoplasmic calcium activates SV currents (Furuichi et al., 2001; Ivashikina and Hedrich, 2005; Ranf et al., 2008; Schulze et al., 2011). On the luminal side, an increase from 0.1 to 1.0 mM calcium inhibits SV channels (Pottosin et al., 2004; Hedrich and Marten, 2011). Screening for mutants impaired in wounding-induced JA biosynthesis identified the *Arabidopsis fou2* mutant (Bonaventure et al., 2007a, 2007b), which harbors a D454N exchange in the SV channel TPC1. The D454N/*fou2* mutant is largely insensitive toward inhibition by vacuolar calcium ions, and *fou2* mesophyll vacuoles accumulate almost twofold higher calcium levels compared with the wild type (Beyhl et al., 2009). This strongly suggests that the luminal calcium sensitivity implemented in TPC1 feeds back on store loading.

Based on structural models, residue Asp-454, which is involved in luminal calcium sensing, is likely located at the inner face of the vacuolar membrane. This notion is underlined by the fact that loss of the negative charge at this position in Fou2/D454N shifts voltage-dependent channel activation by ~30 mV toward less positive vacuole potentials. When compared with the

[1] Address correspondence to gerald.schoenknecht@okstate.edu.
The author responsible for distribution of materials integral to the findings presented in this article in accordance with the policy described in the Instructions for Authors (www.plantcell.org) is: Rainer Hedrich (hedrich@botanik.uni-wuerzburg.de).
[W] Online version contains Web-only data.
www.plantcell.org/cgi/doi/10.1105/tpc.111.086751

wild-type SV channel, the *fou2* mutant channel activates faster and exhibits larger current amplitudes (Bonaventure et al., 2007b; Beyhl et al., 2009). These findings raise questions about the nature of the luminal calcium binding site and how it feeds back to the voltage sensor. Answering this kind of question with plasma membrane ion channels is generally approached through site-directed mutagenesis combined with electrophysiological studies in heterologous expression systems, like *Xenopus laevis* oocytes or animal cell lines (Stühmer et al., 1987; Becker et al., 1996; Geiger et al., 2002). However, most organelle ion channel proteins appear not to be properly incorporated in the plasma membrane of heterologous expression systems (Dunkel et al., 2010).

Thus, applying a homologous expression approach, we answered questions about TPC1 structure and properties with mutated SV channels embedded in their native environment of the vacuolar membrane. To gain insight into the molecular nature of the luminal calcium sensor of the SV channel, we prepared a theoretical three-dimensional (3D) model of TPC1 by homology modeling. This working model was solely used for mutagenesis to predict intravacuolar acidic residues in close proximity to position 454. Site-directed channel mutants were then transiently expressed in *Arabidopsis tpc1-2* protoplasts. Following liberation of vacuoles from transformed protoplast, the calcium dependence of these SV channel mutants was analyzed by patch clamping. Distinct Glu residues in the neighborhood of position 454 could thereby be identified, and their potential to bind luminal calcium and connect the calcium binding site to the channel gate was characterized.

RESULTS

To obtain a hint about the luminal calcium sensor of the SV channel, we aligned TPC1 sequences from different organisms (Figure 1). Upstream of the *fou2* mutation, corresponding to residue Asp-454, a Glu residue is present at position 450 that is conserved among plant and even animal TPCs. Moreover, at positions 456 and 457, all *Arabidopsis* ecotypes contain negatively charged glutamates; however, these two sites are polymorphic in plants. Most available plant sequences exhibit a Glu at the position corresponding to 456 in *Arabidopsis*, and Asn is the prevalent amino acid type at the position corresponding to 457 in TPC1.

Based on hydrophobicity-based predictions (Furuichi et al., 2001) and recent experimental results (Hooper et al., 2011), the TPC1 channel harbors 12 transmembrane domains. This evidence, as well as our theoretical 3D model of TPC1 (Figure 2), suggests that the *fou2* mutation, D454N, is located in a loop between transmembrane domains S7 and S8. Thus, Asp-454 would face the vacuolar lumen, supporting its possible role in contributing to the luminal calcium recognition site of the SV channel. Indeed, no differences between *fou2* and wild-type SV channels were observed in terms of their cytosolic calcium sensitivity (Beyhl et al., 2009). As expected, replacement of a negatively charged Glu by the polar isosteric Gln on the luminal side does not affect the cytosolic EF-hand Ca^{2+} sensor.

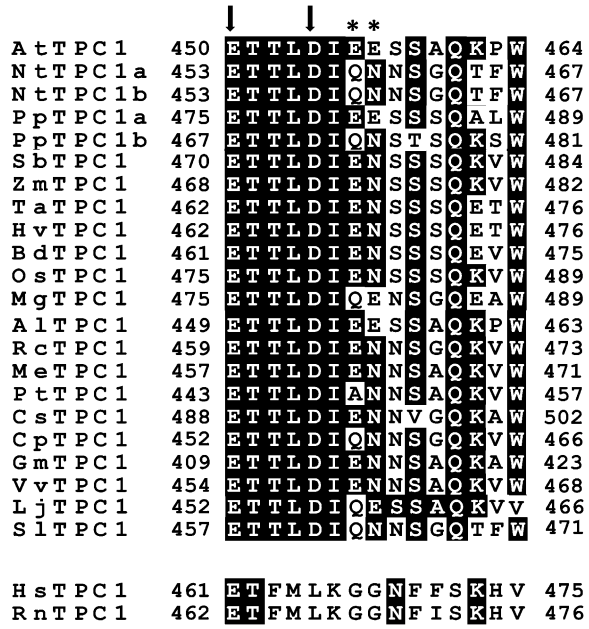

Figure 1. Alignment of the Loop between Transmembrane Domains S7 and S8 of the TPC1 Channel from Different Plant and Animal Species.

The Glu at position 450 (E450, marked by arrow) is conserved in both plant and animal TPC1 sequences, whereas the Asp at position 454 (D454, marked by arrow) is conserved only among plant species. Two polymorphic Glu residues, Glu-456 and Glu-457, are marked by asterisks. TPC1 sequences are from *Arabidopsis thaliana* (At), *N. tabacum* (*Nt*), *P. patens* (*Pp*), *Sorghum bicolor* (Sb), *Zea mays* (Zm), *Triticum aestivum* (Ta), *Hordeum vulgare* (Hv), *Brachypodium distachyon* (Bd), *Oryza sativa* (Os), *Mimulus guttatus* (Mg), *Arabidopsis lyrata* (Al), *Ricinus communis* (Rc), *Manihot esculenta* (Me), *Populus trichocarpa* (Pt), *Cucumis sativus* (Cs), *Carica papaya* (Cp), *Glycine max* (Gm), *Vitis vinifera* (Vv), *Lotus japonicus* (Lj), *Solanum lycopersicum* (Sl), *Homo sapiens* (Hs), and *Rattus norvegicus* (Rn).

Theoretical Modeling Reveals a Novel Calcium Binding Motif at the Luminal Side of TPC1

To obtain molecular insight into the vacuolar calcium sensor, a theoretical 3D model of TPC1 was generated by homology modeling (Figure 2). For this, the *Arabidopsis* sequence was aligned with the sequence of the voltage paddle chimera of the mammalian voltage-dependent K^+ channel Kv1.2 and Kv2.1 of the *Shaker* family, for which a crystal structure is available (PDB entries 2R9R and 2A79) (Long et al., 2005, 2007). As TPC1 consists basically of two Shaker-like domains, each half of the TPC1 amino acid sequence, consisting of six transmembrane helices, according to the TMHMM tool and recent experimental evidence (Hooper et al., 2011), was aligned with the template sequence of the PDB coordinate set 2R9R. The homology model was then obtained by substituting the amino acid residues of Kv1.2-Kv2.1 with those of the aligned TPC1 sequence (see Supplemental Figure 1 online). The N- and C-terminal TPC1 halves were then combined to yield one TPC1 monomer. Subsequently, two TPC1 monomers were structurally aligned onto the tetrameric Kv1.2 assembly, finally providing a functional

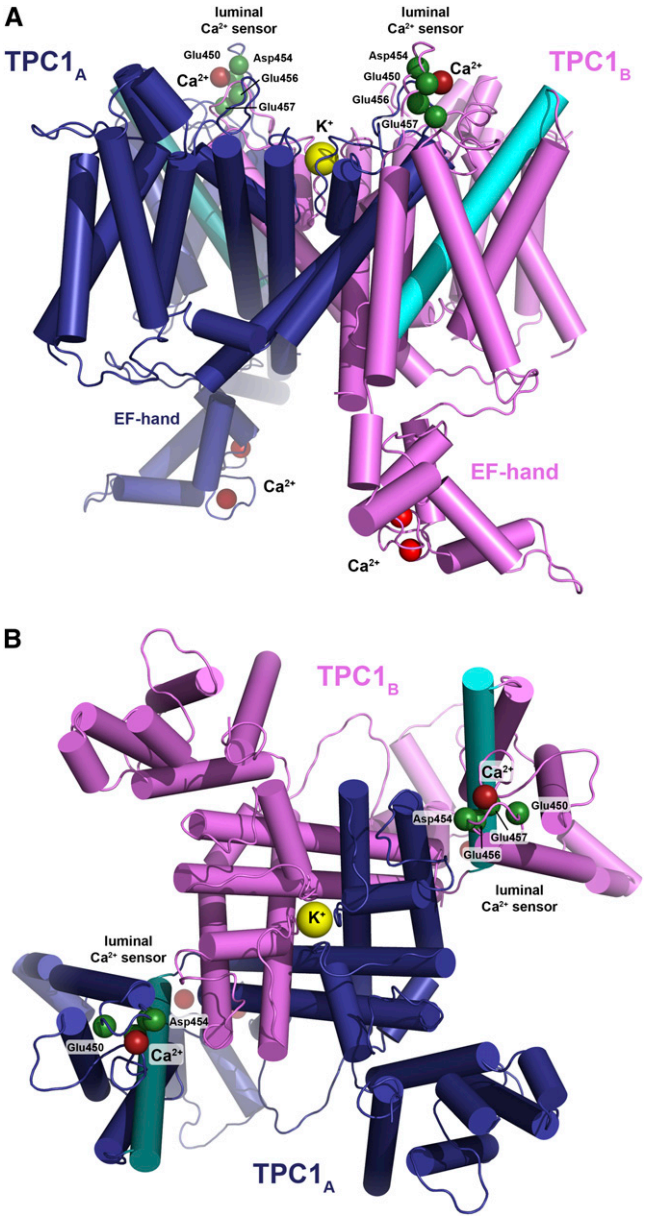

Figure 2. Homology Model of TPC1.

(A) Side view of the overall structure of the transmembrane region of the SV channel in its open conformation. Subunits of the dimeric channel protein are designated by suffixes ($TPC1_A$, dark blue, $TPC1_B$, pink). The voltage-sensing domain S10 in both subunits is colored in cyan. Canonical EF-hands and residues encompassing the luminal calcium sensor facing the cytosolic and vacuolar site, respectively.

(B) Top view of **(A)** from the vacuolar site. Potassium and calcium ions are colored in yellow and red, respectively. The negatively charged Asp (Asp-454) and Glu (Glu-450, Glu-456, and Glu-457) residues investigated here are indicated in green.

TPC1 dimer assembly. Energy minimization and short in vacuo molecular dynamics were performed to remove bad geometry of individual residues or clashes due to van der Waals overlap between side chains of substituted residues. The final model exhibited a good backbone and side chain geometry and has no bad van der Waals contacts (Figure 2).

Based on the *fou2* mutation, the local sequence and structure environment was then analyzed for putative calcium binding motifs. However, no direct structural neighbors or motifs in the sequence showed similarity with known calcium binding motifs. To model a potential Ca^{2+} coordination site around the *fou2* mutation site, Asp-454, we applied a calcium binding EF-hand motif as possible structural template to model the cation coordination site into the loop between transmembrane helices 7 and 8 (Figure 3). The four acidic residues in this loop segment, Glu-450, Asp-454, Glu-456, and Glu-457, were manually aligned onto the residues in the Ca^{2+} binding EF-hand motif of the N-terminal domain of Troponin C (PDB entry 2L1R). A cation coordination arrangement similar to the pentagonal bipyramidal coordination as found in EF-hands could be obtained by manual model building with Glu-450 occupying the position of the conserved first Asp and Asp-454 aligning with the position of the third conserved Asp. While a similar structural arrangement could be modeled, the sequence of the loop residues Glu-450 to Gln-461 of TPC1 differs significantly from the consensus sequence of a canonical EF-hand. However, deviating sequences and loop structures have been reported for calcium binding EF-hand motifs (Gifford et al., 2007). In a canonical EF-hand motif, various positions are almost invariant and usually comprised of the consensus sequence, DXDXDGXIDXXE, with the acidic residues at sequence positions 1, 3, 5, 9, and 12 occupying the +X, +Y, +Z, -X, and -Z calcium coordination sites, respectively (Tufty and Kretsinger, 1975; Kretsinger, 1976). The -Y position of the pentagonal bipyramidal coordination of calcium is provided by a backbone carbonyl and thus does not require a conserved amino acid. In the potential TPC1 luminal calcium binding site, only residue Asp-454 is conserved; however, in our EF-hand like model, the Asp at position 1 is replaced by Glu-450, Thr-452 might functionally replace the Asp at position 3, and the hydroxyl oxygen of Ser-458 might provide for calcium coordination similar to the Asp residue at position 9. The Glu at position 12, which is conserved in a canonical EF-hand, is replaced by an isosteric Gln in our model of the luminal calcium site in TPC1. Thus, the sequence Glu-450 to Gln-461, although not strictly conserved with the amino acid sequence seen in canonical EF-hand motifs, provides acidic residues or oxygen-bearing groups at the positions that can possibly coordinate the divalent calcium cation (Figure 3).

Our model suggests that from the four acidic residues Glu-450, Asp-454, Glu-456, and Glu-457, only the side chains of residues Glu-450 and Asp-454 are directly involved in calcium coordination. Thus, their replacement by other amino acid types should directly affect calcium binding. In the model, the side chain of Glu-456 points toward the protein surface and Glu-457 is involved in stabilizing the loop conformation by forming hydrogen bonds with residues in the C-terminal part of the voltage sensor region S10 (Figure 3). Thus, their replacement might not directly affect calcium binding, but their position

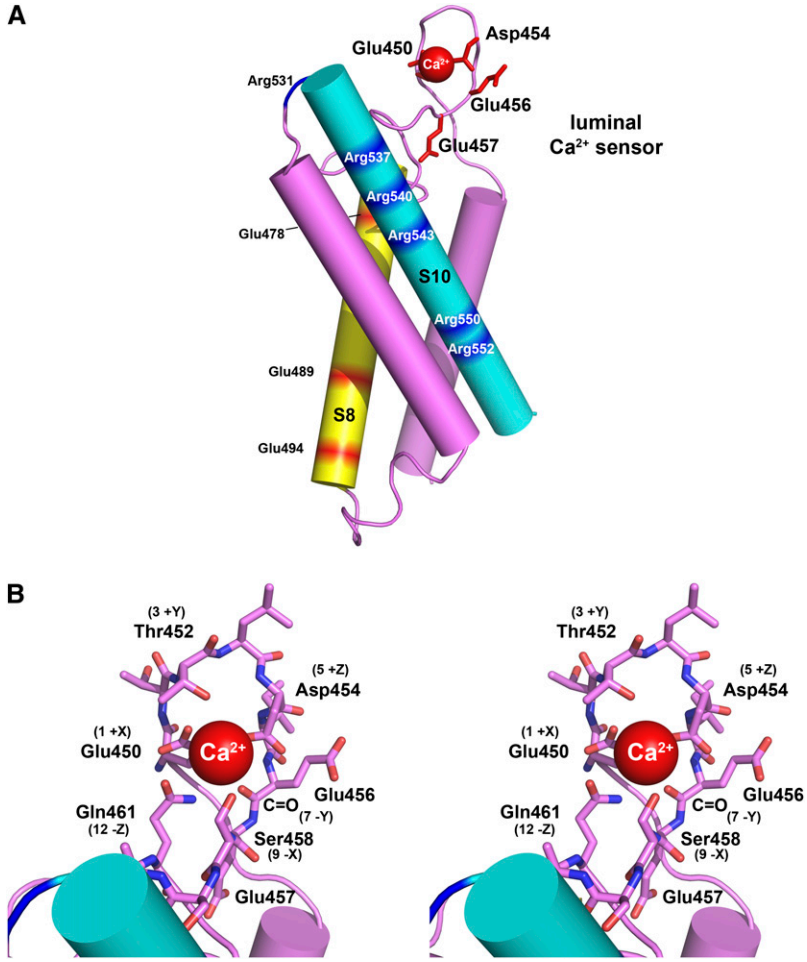

Figure 3. Homology Model of the Proposed Ca^{2+} Binding Site.

(A) Overview: Only the transmembrane elements S7 to S10, which include the voltage sensor, are shown. The two transmembrane elements supposedly interacting during voltage gating, S8 (shown in yellow with acidic residues marked in red) and S10 (cyan with positively charged residues indicated in blue), are shown with the luminal calcium sensor, comprising residues Glu-450, Asp-454, Glu-456, and Glu-457, shown in stick representation.

(B) Stereoview of predicted luminal Ca^{2+} sensor. The loop between transmembrane helices 7 and 8 is shown as a stick representation, showing that the acidic side chains of Glu-450 and Asp-454 are required for calcium coordination, whereas in the case of Glu-456, only the backbone carbonyl is used for ion coordination. The amino acid residues involved in ion coordination are indicated by numbers and their geometric localization with respect to a classical EF-hand.

close to the calcium coordination site could still affect feedback of calcium binding with other regions in the ion channel, such as the voltage sensor.

Standardizing the Expression of *tpc1* Mutants

On the basis of amino acid sequence comparison and the theoretical TPC1 model, we selected individual residues for site-directed mutagenesis to test their impact on luminal calcium sensing. To study the electrical properties resulting from mutations in *TPC1*, we used protoplasts from *tpc1-2* SV channel loss-of-function mutants as a homologous expression system. While SV currents could be elicited already 1 d after transformation, maximal expression levels were observed at day 2.

TPC1 synthesis and insertion into the vacuolar membrane were visualized using green fluorescent protein (GFP) fusion constructs with either wild-type *TPC1* or mutants thereof (Figure 4; see Supplemental Figure 2 online). At day 1, GFP signals were predominately associated with the vacuole and endomembrane structures, whereas at day 2, GFP fluorescence was mainly emitted from the vacuolar membrane, and peak SV current amplitudes could be recorded (see below).

To quantify the expression level of the channel gene, we performed quantitative PCR (qPCR) analyses of protoplast batches transformed with wild-type and mutant *tpc1*. Expression levels of the channel gene were normalized to those of actin. In nontransformed wild-type (Columbia-0 [Col-0]) protoplasts, on average 14,000 *TPC1* transcripts per protoplast were detected

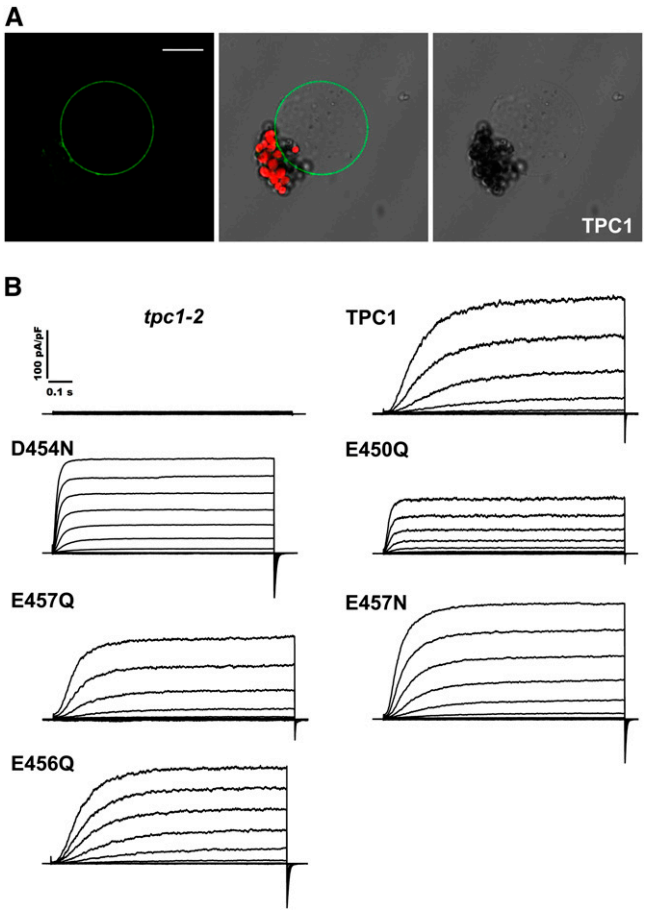

Figure 4. Transformation of *tpc1-2* Protoplasts.

(A) TPC1-GFP green fluorescence and red chlorophyll autofluorescence 48 h after transient transformation in vacuoles released from *tpc1-2* protoplasts. Bar = 10 μm.

(B) Whole vacuolar currents measured in *tpc1-2* nontransformed and transformed knockout plants. The lack of the SV current was complemented 2 d after transient transformation by TPC1 and mutants, and 1000-ms (*tpc1-2*, D454N, E456Q) and 1200-ms (TPC1, E457Q, E457N, E450Q) long pulses were applied in the range from −100 to +110 mV in 15-mV steps from a holding potential of −60 mV. The bath solution (cytosolic side) contained 150 mM KCl, 1 mM $CaCl_2$, and 2 mM DTT, adjusted to pH 7.5 with 10 mM HEPES/Tris. The pipette solution (vacuolar side) comprised 150 mM KCl, 2 mM DTT, 10 mM HEPES/Tris, pH 7.5, 2 mM $MgCl_2$, and 0.1 mM $CaCl_2$.

(see Supplemental Table 1 online). Following transformation of *tpc1-2* protoplasts with wild-type *TPC1*, transcript levels were 60 times higher (see Supplemental Table 2 online). However, compared with Col-0 protoplasts, this increase in *TPC1* mRNA levels did not result in a proportional elevation of the SV current amplitude. This observation is in good agreement with earlier findings (Peiter et al., 2005) that 25- to 30-fold increases in *TPC1* transcript levels are not accompanied by corresponding increases in current amplitudes. This indicates that at 14,000 *TPC1* mRNA copies translation, targeting, and functional assembly of SV channels in *Arabidopsis* mesophyll cells appear to be almost saturated. For *fou2* expression in the *tpc1-2* protoplast system, transcript numbers as high as 1,500,000 (see Supplemental Table 2 online) were detected. However, peak Fou2-SV current amplitudes were only marginally increased compared with those of wild-type TPC1 (Figure 4B). With the other *tpc1* mutants described here, 500,000 to 1,000,000 transcripts could be measured as well, which suggests that we were working at maximal SV channel densities. Recorded current densities (current amplitudes normalized to membrane surface area) varied by about a factor of five, which is comparable to the variability of SV current densities observed in untransformed wild-type *Arabidopsis* mesophyll vacuoles (Schönknecht et al., 2001).

To further test how expression of *tpc1* mutants might affect the vacuolar transport capacity, we analyzed whether overexpression of distinct *tpc1* mutants would alter the transcription levels of vacuolar proton pumps, another major transporter class within the vacuolar membrane. Transcript levels of *Vha-a2* (tonoplast V-ATPase A2), *VHP2;1+2*, and *VHP1;1* (H^+-pyrophosphatases) were similar for wild-type TPC1 and D454N/fou2, E450Q, E456Q, and E457Q mutants (see Supplemental Table 2 online). These results indicate that transient overexpression of wild-type *TPC1* or the mutants in this analysis hardly affected the *Arabidopsis* vacuolar transporter system.

Electrophysiological Characterization of TPC1 Mutants

For patch clamp assessment of the luminal calcium sensitivity of the SV channel, we used 150 mM KCl and 1 mM $CaCl_2$, pH 7.5, in the bath medium (cytosolic side). The pipette solution (vacuolar side) contained 150 mM KCl at pH 7.5. Divalent cation concentrations on the vacuolar side were varied from nominally zero calcium and magnesium (0.1 mM EGTA no $CaCl_2$ or $MgCl_2$ added; 0 Ca/0 Mg) to 2 mM $MgCl_2$ plus 10 mM $CaCl_2$. At a background of 2 mM $MgCl_2$, $CaCl_2$ concentrations were varied from zero (no $CaCl_2$ added; 0 Ca) to 0.1, 1, or 10 mM. Under these conditions, the SV channel operates as strict outward rectifier, mediating cation flow from the cytosolic to the vacuolar side. High cytosolic Ca^{2+} concentrations were chosen to saturate the two cytosolic EF-Ca^{2+} binding motifs, which in turn promotes high SV channel activity (Hedrich and Neher, 1987). The calcium sensitivity of the vacuolar calcium sensor was investigated at a background of 2 mM Mg^{2+}, since it is known that both calcium and magnesium act on the SV channel from the vacuolar side (Pottosin et al., 2004). With submillimolar to low millimolar free Mg^{2+} concentrations inside the vacuole (Shaul, 2002), a background of 2 mM vacuolar Mg^{2+} resembles physiological conditions. Variation of vacuolar Ca^{2+} concentrations from 0.1 to 10 mM covers the extremes of reported vacuolar free Ca^{2+} concentrations (Pottosin and Schönknecht, 2007).

Well in agreement with *TPC1* encoding the SV channel, patch clamp studies with vacuoles released from *tpc1-2* protoplasts demonstrated the lack of major outward rectifying cation currents (Figure 4B) (Peiter et al., 2005; Ranf et al., 2008). Transformation of *tpc1-2* protoplasts with wild-type *TPC1* reconstituted SV-type channel activity (Figure 4B). Whole-vacuole patch clamp recordings on homologously expressed TPC1 displayed the characteristic kinetics of the slow vacuolar channel (Hedrich and Neher, 1987) as recorded with vacuoles from wild-type *Arabidopsis*

plants. When *tpc1-2* protoplasts were transformed with D454N/*fou2*, data from patch clamp recordings were identical to those obtained with vacuoles derived from *fou2* mutant *Arabidopsis* plants (Figure 4B). These results indicate that *tpc1-2* protoplasts provide a reliable homologous expression system to characterize and to perform mutagenesis-based structure function studies on TPC1 luminal calcium sensitivity.

Voltage-dependent activation of SV currents is complex in nature and characterized by a delay. Therefore, one best describes its multiphasic activation kinetics on the basis of activation half-times (Pottosin et al., 2004). Activation kinetics is dependent on the voltage applied. A positive voltage change increases the activation rate, thereby decreasing the activation half-time. With native TPC1, increasing vacuolar Ca^{2+} concentrations cause an increase in the activation half-time and a shift of the voltage-dependent activation to more positive potentials. When compared with the wild-type channel, the voltage- and calcium-dependent activation kinetics of TPC1 mutants exhibited pronounced differences (Figures 5 to 7; see Supplemental Figures 3 and 4 online).

The D454N/*fou2* mutant was characterized as a hyperactive version of the *Arabidopsis* SV channel (Bonaventure et al., 2007b), appearing entirely resistant toward block by vacuolar calcium, in contrast with wild-type TPC1 (Beyhl et al., 2009). Accordingly, when the D454N/*fou2* mutant was expressed in *tpc1-2* protoplasts, SV channel activation shifted to less positive membrane potentials and showed accelerated activation kinetics compared with wild-type TPC1. Neither midpoint potentials nor half-time activation were affected by vacuolar calcium or magnesium (Figures 4B to 7).

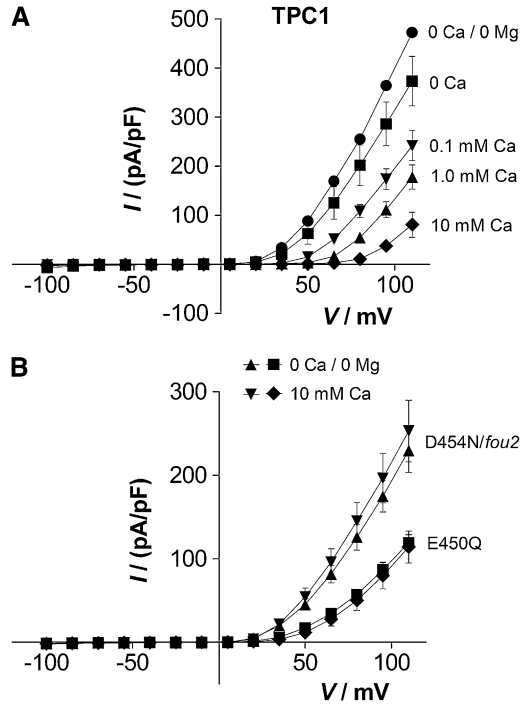

Figure 5. Effect of Luminal Calcium on SV Currents in Mutants and the Wild Type.

Steady state current densities, *I* in pA/pF, recorded at varying voltages, *V* in mV, are plotted for different luminal (vacuolar) Ca^{2+} concentrations. *tpc1-2* protoplasts were transformed transiently by *TPC1* **(A)**, and D454N/*fou2* and E450Q **(B)**. I/V curves evoked upon 15-mV steps in voltages from −100 to +110 mV are presented. The holding potential and the pulse duration were −60 mV and 1000 ms (D454N) or 1200 ms (TPC1, E450Q), respectively. The composition of the bath solution was 150 mM KCl, 1 mM $CaCl_2$, 2 mM DTT, and 10 mM HEPES/Tris, pH 7.5. The pipette solutions contained 150 mM KCl, 2 mM DTT, 10 mM HEPES/Tris, pH 7.5, and various concentrations of divalent cations, namely, 0.1 mM EGTA (no Ca^{2+} or Mg^{2+} added) and 2 mM $MgCl_2$ plus 0, 0.1, 1.0, or 10 mM $CaCl_2$ **(A)** and 2 mM $MgCl_2$ plus 0 or 10 mM $CaCl_2$ **(B)**. All data points were obtained in the second day after transient expression and represent the mean ± SE. The number of measurements was $n = 3$ to 5.

Mutating the Conserved Glu-450 Renders TPC1 Ca^{2+}-Insensitive and Promotes SV Channel Opening

Molecular modeling hypothesized that residue Glu-450 likely participates in the proposed luminal calcium sensor site (Figure 3). We replaced the conserved Glu with Gln and compared the calcium response of this mutant E450Q with the wild-type SV channel and Fou2. Comparable to Fou2, E450Q exhibited very fast activation kinetics (half-time ≤ 50 ms at +60 mV; Figure 7), and, in contrast with the wild type, kinetics were completely insensitive toward changes in vacuolar Ca^{2+} or Mg^{2+}. The activation potential of E450Q was shifted to more positive potentials compared with Fou2, especially midpoint potential V_1, describing the transition between closed state C1 and open state, O. Yet, as for Fou2, the activation potential was not affected by vacuolar Ca^{2+} or Mg^{2+} (Figures 5B and 6), while the activation potential of the native TPC1 shifted toward more positive potentials upon an increase in vacuolar concentrations of these divalent cations (Figure 5A). Thus, the sensitivity of the SV channel toward vacuolar Ca^{2+} and Mg^{2+} is lost in the E450Q mutant, comparable to Fou2 (Figures 5 to 7). The lack of divalent cation sensitivity in both mutants indicates that Asp-454 and Glu-450 represent key components of the luminal calcium sensor.

Mutation of Polymorphic Glu-456 Reduces Calcium Sensitivity, Inhibiting SV Channel Opening

To alter the charge of the two polymorphic Glu residues without changing the geometry of the amino acid side groups, we replaced Glu-456 and -457 in *Arabidopsis* TPC1 with isosteric Gln. Following transformation of *tpc1-2* protoplasts with the *tpc1* mutants E456Q and E457Q, these SV channel mutants were analyzed like Fou2, E450Q, and the wild type. E456Q exhibited decelerated activation kinetics, which were about 2 times slower compared with the wild type (400 ms compared with 220 ms at 0.1 mM Ca^{2+}; Figures 4 and 7). The activation kinetics showed a reduced sensitivity toward vacuolar Ca^{2+} or Mg^{2+}, just displaying a deceleration by about a factor of two when comparing 0 Ca/0 Mg (0.1 mM EGTA no $CaCl_2$ or $MgCl_2$ added) to 10 mM Ca (plus 2 mM Mg^{2+}), in contrast with a five-fold deceleration for wild-type TPC1 (Figure 7). Compared with wild-type TPC1, activation potentials of E456Q were shifted to more positive potentials and were less calcium sensitive. Even at 0 mM Ca^{2+}, midpoint potentials of E456Q resembled wild-type midpoint potentials when Ca^{2+} was added to the

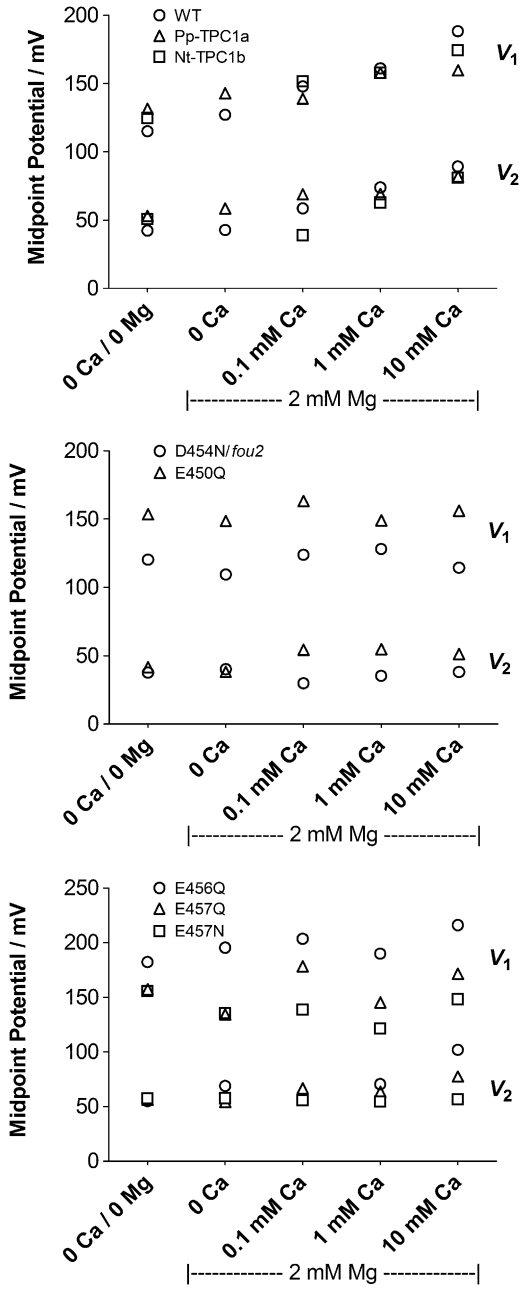

Figure 6. Activation Potentials for Voltage-Dependent Opening of TPC1 Channel Variants.

Whole-vacuole I/V curves were fitted by two Boltzmann distributions to estimate midpoint potentials, V_1 and V_2 (cf. Supplemental Figure 3 online). V_1 describes the voltage-dependent transition between closed state C1 and open state, O, while V_2 describes the transition between the two closed states, C1 and C2. Midpoint potentials are plotted against the concentration of divalent cations applied at the vacuolar side, namely, 0.1 mM EGTA (no Ca^{2+} or Mg^{2+} added) and 2 mM $MgCl_2$ plus 0, 0.1, 1.0, or 10 mM $CaCl_2$.

luminal side (Figure 6). The mutant E456Q showed overall decreased calcium sensitivity (i.e., smaller changes in activation potentials and activation half-times in response to vacuolar divalent cations). In the absence of Ca^{2+}, E456Q exhibited more positive activation potentials and decelerated activation half-times compared with the wild type, indicating a calcium-independent inhibition of SV channel opening by the E456Q mutation.

Mutations in Polymorphic Glu-457 Render TPC Ca^{2+}-Insensitive without Promoting SV Channel Opening

In addition to the isosteric replacement in mutant E457Q, we also tested E457N, since Asn is the prevalent amino acid in plant TPC1 channels at this position (Figure 1). Both E457Q and E457N showed a loss of sensitivity towards luminal divalent cations. Yet, in contrast with D454N/*fou2* and E450Q, which are Ca^{2+}-insensitive as well, E457Q and E457N did not show an accelerated channel opening at less positive potentials. In fact, in the absence of vacuolar Ca^{2+}, E457Q and E457N opened even slower (260 and 280 ms compared with 110 ms for the wild type) and at slightly more positive potentials than wild-type TPC1 did (Figures 6 and 7). Only at increased vacuolar Ca^{2+} levels, when opening of wild-type TPC1 is gradually inhibited, did Ca^{2+}-insensitive TPC1 mutants E457Q and E457N open faster and at less positive potentials compared with the wild type.

Channel Opening of TPC1 from *Physcomitrella* and *Nicotiana*

To gain independent evidence for the function of the polymorphic Glu residues at positions 456 and 457, we expressed TPC1 from *Physcomitrella patens* (Pp-*TPC1a*) and *Nicotiana tabacum* (Nt-*TPC1b*) in *tpc1-2 Arabidopsis* vacuoles for patch clamp analysis. Like At-TPC1, Pp-TPC1a comprises Glu residues at positions 456 and 457, while Nt-TPC1b contains a Gln and an Asn residue, respectively, and, thus, basically resembles an At-TPC1 E456Q/E457N double mutant. Channel opening of Pp-TPC1a is similar to At-TPC1 (see Supplemental Figure 5 online). Activation half-times were almost identical for both species (220 ms for At-TPC1 and 230 ms for Pp-TPC1a at 0.1 mM Ca^{2+}) and showed the same deceleration (from 100 to 600 ms) by luminal divalent cations (Figure 7). The shift to more positive activation potentials at increasing vacuolar Ca^{2+} was comparable for Pp-TPC1a and At-TPC1 (Figure 6). Like Pp-TPC1a and At-TPC1, Nt-TPC1b showed a shift of activation potentials to more positive values upon increasing vacuolar Ca^{2+} and Mg^{2+} concentrations (Figure 6). However, activation half-times were very long (1 to 2 s; see Supplemental Figure 6 online) and did not show any sensitivity toward luminal divalent cations. These long activation half-times did not even show the typical voltage dependence observed in all other TPC1 channel variants tested here (Figure 7; see Supplemental Figure 4 online). Compared with wild-type At-TPC1, both mutants, E456Q and E457N, show prolonged activation half-times. One could speculate that in Nt-TPC1b the combination of both mutant features resulted in the observed extremely long activation times.

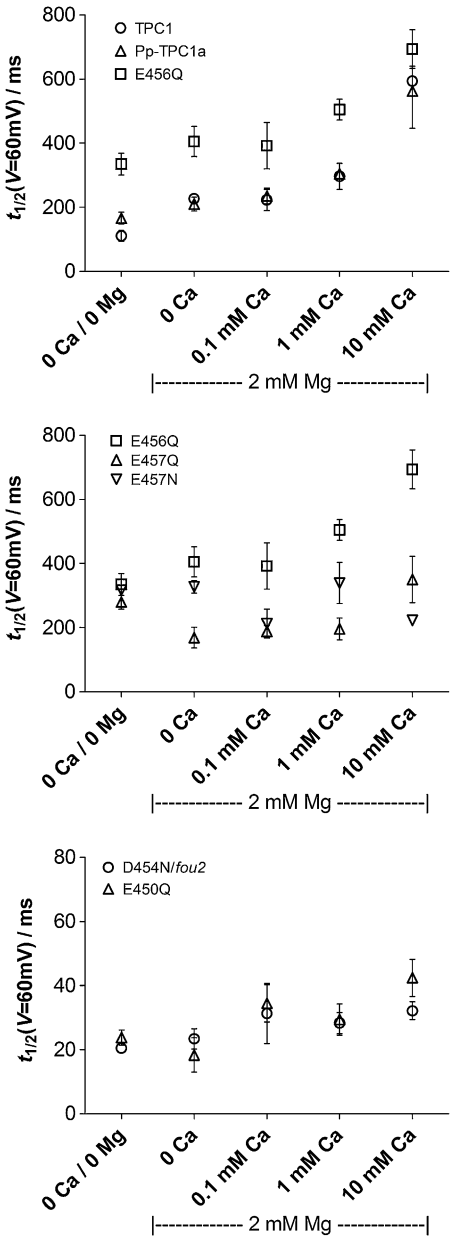

Figure 7. Activation Half-Times of TPC1 Channel Variants.

Mean activation half-times (±95% confidence interval) at +60 mV, $t_{1/2}(V$ = 60 mV), were calculated from monoexponential fits of the voltage dependence of activation half-times [$t_{1/2}$ = f(V); cf. Supplemental Figure 4 online]. For comparison, the data set for E456Q was included in both top plots. Please note that the y axis of the bottom plot differs by a factor of 10 compared with the top two plots. Activation half-times are plotted against the concentration of divalent cations applied at the vacuolar side, namely, 0.1 mM EGTA (no Ca^{2+} or Mg^{2+} added) and 2 mM $MgCl_2$ plus 0, 0.1, 1.0, or 10 mM $CaCl_2$.

DISCUSSION

Calcium-based signaling networks are central to plants' responses to abiotic and biotic stresses. Changes in cytosolic calcium concentrations are decoded by, for example, calcium-dependent kinases, calcineurin B–like proteins, or calmodulin. In these proteins, EF-hands represent a common structural motif capable of binding calcium ions originating from extracytosolic sources, such as the cell wall/apoplast (extracellular) or organelles (intracellular). Despite varying extracellular Ca^{2+} concentrations ($[Ca^{2+}]_{ext}$) plant cells maintain homeostasis of cytosolic free Ca^{2+} concentrations ($[Ca^{2+}]_{cyt}$) around 10^{-7} M. In *Arabidopsis* guard cells, the regulatory mechanisms for $[Ca^{2+}]_{cyt}$ homeostasis involve the CAS (Ca^{2+} sensing receptor) protein (Han et al., 2003). Acidic amino acids in the CAS protein are predicted to constitute a low-affinity Ca^{2+} binding region distinct from high-affinity EF-hands. Since CAS represents an integral thylakoid membrane protein, chloroplasts seem to participate in $[Ca^{2+}]_{ext}$-induced $[Ca^{2+}]_{cyt}$ transients and stomatal closure (Nomura et al., 2008; Weinl et al., 2008). Besides chloroplasts, vacuoles are postulated to represent important calcium stores. However, little is known about the dynamics of vacuolar calcium storage or the molecular mechanisms that regulate calcium homeostasis across the vacuolar membrane. The SV channel represents the major vacuolar conductance for cations and is activated by cytosolic Ca^{2+} and blocked by elevated luminal levels of the signaling cation (Hedrich and Marten, 2011, and references therein).

Following up on the observation that a point mutation (D454N) in TPC1 eliminated sensitivity to vacuolar Ca^{2+} and altered the vacuolar calcium content (Beyhl et al., 2009), here, we characterized the luminal calcium sensor of the SV channel. Polymorphism analyses and structural modeling identified an array of negatively charged residues representing a potential calcium binding site in the connecting loop of transmembrane helices S7 and S8 (Figures 2 and 3). Site-directed mutagenesis of residues in close proximity to position Asp-454 combined with patch clamping indicated that Glu-450, Glu-456, and Glu-457 contribute to SV channel inhibition by luminal calcium. Mutations of the conserved Asp-454 as well as the proximal Glu-450 resulted in complete loss of sensitivity toward luminal calcium or magnesium ions. In these mutants, SV channel opening was very fast (half-times of 20 to 30 ms at +60 mV) and required relatively small potentials, indicating a low energy barrier. The two conserved negative amino acids, Asp-454 and Glu-450, are essential for TPC1 modulation by luminal divalent cations and according to our theoretical 3D model are directly involved in Ca^{2+}/Mg^{2+} binding. Mutations in the two distal polymorphic Glu residues at positions 456 and 457 had a different effect. Again, calcium sensitivity of SV channel opening was significantly reduced, but activation potentials were higher, and opening kinetics were slowed down (half-times of 200 to 300 ms at +60 mV). This indicated an increased energy barrier for channel opening, even though channel opening was hardly affected by luminal divalent cations.

How Does Binding of Luminal Calcium Regulate SV Channel Gating?

To understand how luminal calcium or magnesium regulate SV channel gating, it is helpful to compare the results presented

here with earlier biophysical characterizations of the SV channel (Pottosin et al., 2004). The analysis of patch clamp recordings on *Beta vulgaris* tap root vacuoles identified two different binding sites for luminal divalent cations. A voltage-dependent reduction in single-channel conductance indicates that divalent cations block the permeation pathway of the SV channel by binding within the channel pore. In addition, a Ca^{2+}-selective binding site outside the membrane spanning part of the channel at the luminal side was characterized. Binding of divalent cations to this luminal site stabilizes the channel's closed conformations, shifting activation potentials to more positive potentials and slowing down channel opening kinetics (Pottosin et al., 2004). It is this luminal binding site that was modified in the TPC1 mutants studied here. Mutations in Asp-450 or Glu-454 eliminated Ca^{2+}-dependent stabilization of TPC1 in its closed conformation, reducing the energy barrier for channel opening and allowing faster channel opening at lower potentials. This effect is expected if Ca^{2+} can no longer bind to the luminal side of TPC1 in E450Q and D454N.

The TPC1 3D model presented here (Figures 2 and 3) is based on the crystallographic structure of a voltage-dependent K^+ (Kv) channel in its open conformation (Long et al., 2007). In the open conformation, the luminal Ca^{2+} binding site of the SV channel has a reduced affinity for both Ca^{2+} (90 μM) and Mg^{2+} (1.6 mM) compared with the closed conformation that binds Ca^{2+} (3 to 4 μM) and Mg^{2+} (64 μM for C2 and 470 μM for C1) with higher affinities (Pottosin et al., 2004). This seems to be in line with the low-affinity Ca^{2+} binding predicted by the homology model for the luminal Ca^{2+} binding site. Both the homology model (Figure 3) and the electrophysiological characterization of single point mutants (Figures 4 to 7) suggest that the conserved Glu-450 and Asp-454 are part of the luminal binding site for divalent cations. Remarkably, these sites are invariable in all plant TPC1 sequences so far available and compared here. It is thus tempting to speculate that SV channels from moss to higher plants exhibit the basic luminal Ca^{2+}sensitivity initially characterized in the beet root SV channel homolog of TPC1 by Pottosin et al. (2004).

How Does the Calcium Binding Site Interact with the Channel Gate?

In contrast with the two invariable sites, the two polymorphic Glu residues at positions 456 and 457 do not seem to be directly involved in calcium binding. This is indicated by both our homology model (Figures 2 and 3) and the electrophysiological characterization of point mutants (Figures 4 to 7). If not directly involved in calcium binding, how can the effects observed for E456Q, E457Q, and E457N be explained? Mutations of either Glu-456 or Glu-457 stabilized the closed conformation of the channel (i.e., slow opening at higher potentials) and at the same time uncoupled channel gating from luminal Ca^{2+} binding. This could indicate that Glu-456 and Glu-457 are involved in the interaction between the luminal calcium binding site and channel gate. Mutations in amino acid residues connecting the calcium binding site and channel gate are likely to uncouple gating from calcium binding, and mutations in amino acids that interact with the channel gate are likely to stabilize the channel in a certain conformation. According to our homology model (Figures 2 and 3), Glu-456 and Glu-457 are in close proximity to the S10 voltage sensor domain. Transmembrane voltage is sensed by positive charges in the membrane-spanning voltage sensor. In *Shaker*-type K^+ channels, membrane potential changes result in movement of the voltage sensor domain, causing the channel gate to open (Catterall, 2010; Cui, 2010). Given a similar gating mechanism in TPC1, interaction of Glu-456 and Glu-457 with the N-terminal region (S9-S10 connecting loop) of the S10 voltage sensor domain could stabilize the closed conformation of the SV channel.

In other voltage-dependent K^+ channels, the modulation of voltage-dependent channel opening by Ca^{2+} has been characterized. Comparable to TPC1, in HERG channels, small changes in external calcium concentration shift the voltage dependence of channel activation to more positive membrane potentials without affecting gating charge. Using site-directed mutagenesis, two adjacent negatively charged amino acids in the S3-S4 linker, near the S4 voltage sensor of the HERG channel, were identified as participating in low-affinity binding sites that regulate voltage and Ca^{2+} dependence of the channel (Johnson et al., 2001; Hofer, 2005). To refine our model, future mutagenesis studies will have to explore whether TPC1 sites related to those that govern HERG gating are addressed via Glu-456 and Glu-457.

Final Considerations in Light of Plant Evolution

To explain the effects of luminal calcium on the gating behavior of TPC1, we compared biophysical data from *B. vulgaris* tap roots (Pottosin et al., 2004) with those from *Arabidopsis* mesophyll cells presented here. Is this a reasonable approach? We think so, since TPC1 seems to be highly conserved among all land plants. The *P. patens* SV channel is surprisingly similar to the *Arabidopsis* SV channel even though *Tracheophyta* and *Bryophyta* split apart almost 600 million years ago (Lang et al., 2008; Magallon and Hilu, 2009). Neither activation potential nor half activation times differ significantly between *Physcomitrella* and *Arabidopsis* (see Supplemental Figures 3 and 4 online), revealing a high degree of conservation in the SV channel characteristics. Moreover, the data for 2 mM Mg^{2+} from Pottosin et al. (2004) nicely correlate with the 0 Ca (plus 2 mM Mg^{2+}) data presented here.

The fact that Glu-450 and Asp-454 are conserved, while Glu-456 and Glu-457 are not, nicely fits the different functions we could assign to those residues here. Glu-450 and Asp-454 are predicted to be parts of the luminal calcium binding domain and directly interact with the Ca^{2+} ion. To bind Ca^{2+}, negative charges are needed; therefore, it is to be expected that amino acid side chains that directly interact with Ca^{2+} are conserved. By contrast, for Glu-456 and Glu-457, we assume that they do not directly interact with Ca^{2+} but are involved in connecting the calcium binding site to the channel gate. Accordingly, one would expect more flexibility to allow for mutations in amino acid side chains that transmit the inhibitory effect from the Ca^{2+} binding site to the voltage-sensing domain, since a mutation can be easily compensated by a mutation in the interaction partner.

Our results provide evidence for a role for TPC1 as part of a novel vacuolar calcium sensing machinery that is based on a non-EF-hand, acidic amino acid array on the molecular level. Apart from the CAS protein, the TPC1 channel thus constitutes

an additional element to monitor extracytosolic Ca^{2+} in plant cells. Future studies will have to show whether the vacuolar calcium site of TPC1 proteins could represent a potential target to address the calcium storage capacity of plants.

METHODS

Plant Material and Growth Conditions

Arabidopsis thaliana ecotype Col-0, *fou2* (Bonaventure et al., 2007b), and the *tpc1-2* mutant (Peiter et al., 2005) were grown on soil in a growth chamber under 8/16 h (short day), 22/16°C conditions and a photon flux density of 150 $\mu mol \cdot m^{-2} \cdot s^{-1}$.

Cloning Procedures

Pp-*TPC1a* was amplified from sterile gametophyte cDNA of cultured *Physcomitrella patens*. *TPC1* clones from *Arabidopsis*, *Physcomitrella* (Pp-*TPC1a*), and tobacco (*Nicotiana tabacum*; Nt-*TPC1b*) (Kadota et al., 2004) were cloned as C-terminal *EGFP* fusions into a modified pSAT6-EGFP-C1 expression vector (GenBank AY818377.1) by an advanced uracil-excision-based cloning technique (Nour-Eldin et al., 2010). This resulted in *EGFP-AtTPC1*/pSAT, *EGFP-PpTPC1a*/pSAT, and *EGFP-NtTPC1b*/pSAT. Primers used for Pp-*TPC1a* were forward 5′- GTTTTTTGGATAAGCTTCAATGC-3′ and reverse 5′-CTCTTTTCTGTTCATCAAGAAGATTG-3′ and for Nt-*TPC1b* were forward 5′-GGCTTAAUATGGAAGAATATCTACTGTC-3′ and reverse 5′-GGTTTAAUTTATGGATTCTCATTGGAGC-3′.

Site-Directed Mutagenesis

Point mutations were introduced into *TPC1* cDNA by means of a modified USER fusion method (Nørholm, 2010). In brief, *TPC1*/pSAT was used as a template for USER mutagenesis and overlapping primer pairs (covering 8 to 11 bp of the mutagenesis site) carrying the desired mutation at their respective 5-prime end were designed according to Supplemental Figure 7 online. The only requirement for USER-based mutagenesis is an adenosine (A) at the 5′ and a thymidine (T) 8-11 bp downstream of the desired fusion product. The site of mutagenesis should be located within this tail region. The first T residue in the tail region of the desired USER primer has to be replaced by uracil (U). PCR conditions were essentially as described by Nørholm (2010) using PfuX7 polymerase. PCR products were treated with the USER enzyme (NEB) to remove the uracil residues, generating single-stranded overlapping ends. Following uracil excision, recirculation of the plasmid was performed at room temperature for 30 min, and constructs were immediately transformed into chemical-competent *Escherichia coli* cells. All mutants were verified by sequencing. Primer sequences are provided in Supplemental Table 3 online.

Transient Expression Procedure and Imaging

Functional expression of TPC1 channels in *Arabidopsis* mesophyll protoplasts, isolated from 6- to 7-week-old *tpc1-2* plants, was achieved by transient expression (Sheen, 2002; Yoo et al., 2007). For imaging, vacuoles were released from transformed protoplasts 24 or 48 h after transformation using standard bath solution (see below). EGFP-tagged TPC1 constructs allowed monitoring of expression. Protoplasts were imaged using a confocal laser scanning microscope (LSM 5 Pascal; Zeiss) under a ×40 Plan-Apochromat water immersion objective.

Real-Time qPCR

Mesophyll protoplasts were isolated as described above, and mRNA was purified twice using a Dynabeads mRNA direct kit (Dynal) according to the manufacturer's instructions. First-strand cDNA was prepared using the M-MLV-RT kit (Promega) and diluted for qPCR 20-fold in water. Quantification and calculation of actin and marker transcripts were performed by real-time PCR as described previously (Ivashikina et al., 2003) using the ABsolute SYBR Capillary Mix (ABgene). The following primers were used: *ACT2/8*fwd (5′-GGTGATGGTGTGTCT-3′), *ACT2/8*rev (5′-ACTGAGCACAATGTTAC-3′), *TPC1*fwd (5′-CTGTGTATCTACTGCTC-3′), *TPC*1rev 5′-ACGAAATATGTAATGCTC-3′), *VHP2;1+2*fwd (5′-TTTAGTGCG TATATGGAC-3′),*VHP2;1+2*rev (5′-CTTCTTACTTCGTTGACA-3′), *VHP1;1*fwd (5′-CAGTATATTCGTTAGCTT-3′), *VHP1;1*rev (5′-TGATAACTTTAGGGGTC-3′), *VHA-a2*fwd (5′-TGTTCCGATGTATCAGA-3′), and *VHA-a2*rev (5′-CAAATGGGAATTTTACCT-3′).

Electrophysiology

Patch clamp experiments on vacuoles were performed at day 2 after transformation in the whole vacuole configuration as described (Beyhl et al., 2009). Release of vacuoles from transformed protoplasts was achieved by incubation in 5× diluted W5 buffer (Sheen, 2002; Yoo et al., 2007) for 8 min. Resistance of patch pipettes, prepared from Kimax-51 glass capillaries (Kimble Products), was ~3 MΩ. Macroscopic currents were recorded at an acquisition rate of 500 μs with an EPC9 patch clamp amplifier (HEKA Electronic) and low-pass filtered at 2.9 kHz. Data were analyzed offline using the software programs Pulse (HEKA Electronic) and IGORPro (Wave Metrics). The standard bath solution (cytosolic side) was composed of 150 mM KCl, 1 mM $CaCl_2$, and 2 mM DTT, adjusted to pH 7.5 with 10 mM HEPES/Tris and set to an osmolarity of 310 $mOsmol \cdot kg^{-1}$ with D-sorbitol. The pipette solution (vacuolar side) contained 150 mM KCl, 2 mM DTT, 10 mM HEPES/Tris, pH 7.5, and an osmolarity of 310 $mOsmol \cdot kg^{-1}$ adjusted with D-sorbitol. Various concentrations of divalent cations were used as follows: 0.1 mM EGTA (no $CaCl_2$ or $MgCl_2$ added), 0.1 mM EGTA and 2 mM $MgCl_2$ (no $CaCl_2$ added), and 2 mM $MgCl_2$ plus three different $CaCl_2$ concentrations (i.e., 0.1, 1, and 10 mM). Free Ca^{2+} concentrations for the pipette and bath media were calculated with WEBMAXC standard (http://www.stanford.edu/~cpatton/webmaxc/webmaxcS.htm). Details of the composition of the solutions are given in the figure legends.

Modeling of TPC1

Alignments were performed using ClustalW (http://www.genome.jp/tools/clustalw/) and BOXSHADE 3.21 (http://www.ch.embnet.org/software/BOX_form.html). A homology model of *Arabidopsis* TPC1 was derived from the crystal structure of a chimeric voltage-dependent K^+ channel in which the voltage-sensor paddle had been transferred from Kv2.1 to Kv1.2 (Long et al., 2005, 2007). The 12 transmembrane helices of TPC1 were predicted from the amino acid sequence using the TMHMM Server. As TPC1 presents a dimeric assembly of two Shaker-like domains, the sequence of TPC1 was separated into the N- and C-terminal half (each comprising six predicted transmembrane helices, residues Ser-60 to Glu-310 and Pro-430 to Asp-680), and both halves were aligned to the sequences of the voltage paddle chimera of the mammalian voltage-dependent K^+ channels Kv1.2 and Kv2.1 of the *Shaker* family (PDB entries 2R9R and 2A79). Manual editing was performed to shift insertions and deletions within the transmembrane helices to the loop regions whenever possible. A first preliminary model was built by exchanging residues of either channel structures with the corresponding residues in TPC1. Bad van der Waals contacts between modeled side chains were then removed by a first round of rotamer searches using the X-Build tool of Quanta2008. Amino acid sequence deletions and insertions were built manually; backbone conformations for those regions were constrained to comply with the Ramachandran rules when possible. After these manual rebuilding procedures, the TPC1 model was submitted to several iterative energy refinement steps. First, only side

chains were released with a weak harmonic potential (k_{pot} = 2 kcal mol^{-1} Å^{-2}), but the protein backbone was kept fixed. After 500 steps of energy minimization, the strict backbone atom constrains were released and backbone atoms were restrained with a harmonic potential of 50 kcal mol^{-1} Å^{-2}. This procedure was repeated twice and the restraints on the backbone atoms were decreased stepwise to 5 kcal mol^{-1} Å^{-2}. By this procedure, changes in the structure were mainly introduced in the side chain positions, whereas the protein backbone movements were minimal. Analysis of the dimeric TPC1 assembly using the tool RAMPAGE yields that 98% of the residues exhibit backbone torsion angles in the favored or allowed region of the Ramachandran plot, thereby indicating the good backbone geometry of the final model.

To model the luminal calcium sensor in TPC1, the sequence from Ile-445 to Ile-474, located between the transmembrane helices 7 and 8, were manually aligned onto the sequence of the EF-hand of Troponin C (PDB entry 2L1R; (Robertson et al., 2010) with Glu-450 aligning onto the first Asp residue of the EF-hand occupying the +X position Asp-65. With this placement, Asp-454 of TPC1 would then be positioned at position 5 and coordinating the Ca^{2+} ion in the +Z position. The side chain carboxylate group of Glu-456 and -457 would be facing away from the cation, and only the backbone carbonyl of Glu-456 would be part of the pentagonal bipyramidal coordination. Modeling of the calcium coordination loop was completed by energy minimization with the calcium ion kept fixed and gradually removing harmonic potential restraints with the side chains (25, 10, and 2 kcal mol^{-1} Å^{-2}) exhibiting weaker restraints than backbone atoms (50, 25, and 5 kcal mol^{-1} Å^{-2}) to maintain the loop backbone conformation. To test for the conformational stability of the coordination loop, a molecular dynamics simulation comprising of 0.5 ns in explicit water was performed. First, the loop comprising of residues Ile-454 to Ile-474 was placed in a rectangular water box of 50 $\times$ 50 $\times$ 50 Å^3 consisting of 2844 solvent molecules and harboring a total of 9005 atoms. The all-hydrogen force field CHARMM22 was used, a van der Waals nonbonded cutoff of 15 Å was used, and the water box was maintained by periodic boundaries around the box, all simulations were done with a time step of 1 fs at a constant temperature of 300K. First, the solvent molecules were relaxed by short molecular dynamics (MD) runs (100 ps) with only the solvent molecules liberated, and then the peptide loop (gradually by keeping backbone atoms restrained more than side chain atoms) was further minimized by several 100- to 200-ps MD runs for equilibration of the system. For the final MD simulation, 0.5 ns of free dynamics (only the calcium atom was fixed in the center of the box to avoid movements of the peptide loop within the water box) was performed. The total energy of the system leveled at $-59{,}500 \pm 800$ kcal mol^{-1}. The energies for bonds, angles, van der Waals, and electrostatic interactions were at $90 \pm 10, 270 \pm 50$, -1700 ± 200 (Lennart-Jones potential for van der Waals interactions), and $-58{,}200 \pm 900$ kcal mol^{-1}, respectively, indicating that the system had reached equilibrium. Starting and final conformation showed a low root mean square deviation for the backbone atoms of 0.96 Å (and only 1.1 Å for all heavy atoms), indicating that the modeling of the calcium coordination loop into an EF-hand-like structure is not achieved by overconstraining the loop.

Accession Numbers

TPC1 sequences were obtained either from the National Center for Biotechnology Information or Phytozome (http://www.phytozome.net/) by BLAST searches. Sequence data from this article can be found in the Arabidopsis Genome Initiative or GenBank/EMBL databases under the accession numbers listed in Supplemental Table 4 online.

Supplemental Data

The following materials are available in the online version of this article.

Supplemental Figure 1. Alignment of At-TPC1 Half-Channels to the Transmembrane Region of the Shaker Kv1.2-Kv2.1 Paddle Chimera Channel.

Supplemental Figure 2. Transformation of *tpc1-2* Protoplasts.

Supplemental Figure 3. Voltage-Dependent Activation of the TPC1 Channel Variants.

Supplemental Figure 4. Activation Half-Times of the TPC1 Channel Variants.

Supplemental Figure 5. Pp-TPC1a Expressed Transiently in *tpc1-2* Protoplasts.

Supplemental Figure 6. Nt-TPC1b Expressed Transiently in *tpc1-2* Protoplasts.

Supplemental Figure 7. Introduction of Point Mutations into cDNA by Means of a Modified USER Fusion Method (Nørholm, 2010).

Supplemental Table 1. qRT-PCR of Nontransformed Protoplasts.

Supplemental Table 2. qRT-PCR of Transformed Protoplasts.

Supplemental Table 3. Primers Used.

Supplemental Table 4. Accession Numbers.

ACKNOWLEDGMENTS

This work was supported by the Deutsche Forschungsgemeinschaft through SFB 487 and FOR964 (R.H.) and by the National Science Foundation through Grant 0925298 (G.S.).

Received April 28, 2011; revised June 21, 2011; accepted July 5, 2011; published July 15, 2011.

REFERENCES

Becker, D., Dreyer, I., Hoth, S., Reid, J.D., Busch, H., Lehnen, M., Palme, K., and Hedrich, R. (1996). Changes in voltage activation, Cs^+ sensitivity, and ion permeability in H5 mutants of the plant K^+ channel KAT1. Proc. Natl. Acad. Sci. USA **93:** 8123–8128.

Bethmann, B., Thaler, M., Simonis, W., and Schönknecht, G. (1995). Electrochemical potential gradients of H^+, K^+, Ca^{2+}, and Cl^- across the tonoplast of the green alga *Eremosphaera viridis.* Plant Physiol. **109:** 1317–1326.

Beyhl, D., Hörtensteiner, S., Martinoia, E., Farmer, E.E., Fromm, J., Marten, I., and Hedrich, R. (2009). The fou2 mutation in the major vacuolar cation channel TPC1 confers tolerance to inhibitory luminal calcium. Plant J. **58:** 715–723.

Bonaventure, G., Gfeller, A., Proebsting, W.M., Hörtensteiner, S., Chételat, A., Martinoia, E., and Farmer, E.E. (2007b). A gain-of-function allele of TPC1 activates oxylipin biogenesis after leaf wounding in Arabidopsis. Plant J. **49:** 889–898.

Bonaventure, G., Gfeller, A., Rodríguez, V.M., Armand, F., and Farmer, E.E. (2007a). The *fou2* gain-of-function allele and the wild-type allele of *Two Pore Channel 1* contribute to different extents or by different mechanisms to defense gene expression in Arabidopsis. Plant Cell Physiol. **48:** 1775–1789.

Catterall, W.A. (2010). Ion channel voltage sensors: Structure, function, and pathophysiology. Neuron **67:** 915–928.

Cui, J. (2010). BK-type calcium-activated potassium channels: Coupling of metal ions and voltage sensing. J. Physiol. **588:** 4651–4658.

Dodd, A.N., Kudla, J., and Sanders, D. (2010). The language of calcium signaling. Annu. Rev. Plant Biol. **61:** 593–620.

Dunkel, M., Müller, T., Hedrich, R., and Geiger, D. (2010). K^+ transport characteristics of the plasma membrane tandem-pore channel TPK4 and pore chimeras with its vacuolar homologs. FEBS Lett. **584:** 2433–2439.

Furuichi, T., Cunningham, K.W., and Muto, S. (2001). A putative two pore channel AtTPC1 mediates $Ca^{(2+)}$ flux in *Arabidopsis* leaf cells. Plant Cell Physiol. **42:** 900–905.

Geiger, D., Becker, D., Lacombe, B., and Hedrich, R. (2002). Outer pore residues control the $H^{(+)}$ and $K^{(+)}$ sensitivity of the *Arabidopsis* potassium channel AKT3. Plant Cell **14:** 1859–1868.

Geiger, D., Scherzer, S., Mumm, P., Marten, I., Ache, P., Matschi, S., Liese, A., Wellmann, C., Al-Rasheid, K.A.S., Grill, E., Romeis, T., and Hedrich, R. (2010). Guard cell anion channel SLAC1 is regulated by CDPK protein kinases with distinct Ca^{2+} affinities. Proc. Natl. Acad. Sci. USA **107:** 8023–8028.

Gifford, J.L., Walsh, M.P., and Vogel, H.J. (2007). Structures and metal-ion-binding properties of the Ca^{2+}-binding helix-loop-helix EF-hand motifs. Biochem. J. **405:** 199–221.

Han, S., Tang, R., Anderson, L.K., Woerner, T.E., and Pei, Z.-M. (2003). A cell surface receptor mediates extracellular Ca^{2+} sensing in guard cells. Nature **435:** 196–200.

Hedrich, R., and Marten, I. (2011). TPC1 – SV channels gain shape. Mol. Plant **4:** 428–441.

Hedrich, R., and Neher, E. (1987). Cytoplasmic calcium regulates voltage-dependent ion channels in plant vacuoles. Nature **329:** 833–835.

Hetherington, A.M., and Brownlee, C. (2004). The generation of $Ca^{(2+)}$ signals in plants. Annu. Rev. Plant Biol. **55:** 401–427.

Hofer, A.M. (2005). Another dimension to calcium signaling: A look at extracellular calcium. J. Cell Sci. **118:** 855–862.

Hooper, R., Churamani, D., Brailoiu, E., Taylor, C.W., and Patel, S. (2011). Membrane topology of NAADP-sensitive two-pore channels and their regulation by N-linked glycosylation. J. Biol. Chem. **286:** 9141–9149.

Ivashikina, N., Deeken, R., Ache, P., Kranz, E., Pommerrenig, B., Sauer, N., and Hedrich, R. (2003). Isolation of *AtSUC2* promoter-GFP-marked companion cells for patch-clamp studies and expression profiling. Plant J. **36:** 931–945.

Ivashikina, N., and Hedrich, R. (2005). K^+ currents through SV-type vacuolar channels are sensitive to elevated luminal sodium levels. Plant J. **41:** 606–614.

Johnson, J.P., Jr., Balser, J.R., and Bennett, P.B. (2001). A novel extracellular calcium sensing mechanism in voltage-gated potassium ion channels. J. Neurosci. **21:** 4143–4153.

Kadota, Y., Furuichi, T., Ogasawara, Y., Goh, T., Higashi, K., Muto, S., and Kuchitsu, K. (2004). Identification of putative voltage-dependent Ca^{2+}-permeable channels involved in cryptogein-induced Ca^{2+} transients and defense responses in tobacco BY-2 cells. Biochem. Biophys. Res. Commun. **317:** 823–830.

Kretsinger, R.H. (1976). Calcium-binding proteins. Annu. Rev. Biochem. **45:** 239–266.

Lang, D., Zimmer, A.D., Rensing, S.A., and Reski, R. (2008). Exploring plant biodiversity: The Physcomitrella genome and beyond. Trends Plant Sci. **13:** 542–549.

Long, S.B., Campbell, E.B., and Mackinnon, R. (2005). Voltage sensor of Kv1.2: structural basis of electromechanical coupling. Science **309:** 903–908.

Long, S.B., Tao, X., Campbell, E.B., and MacKinnon, R. (2007). Atomic structure of a voltage-dependent K^+ channel in a lipid membrane-like environment. Nature **450:** 376–382.

Magallon, S., and Hilu, K.W. (2009). Land plants (Embryophyta). In The Timetree of Life, S.B. Hedges and S. Kumar, eds (Oxford, UK: Oxford University Press), pp. 133–137.

Nomura, H., Komori, T., Kobori, M., Nakahira, Y., and Shiina, T. (2008). Evidence for chloroplast control of external Ca^{2+}-induced cytosolic Ca^{2+} transients and stomatal closure. Plant J. **53:** 988–998.

Nørholm, M.H. (2010). A mutant Pfu DNA polymerase designed for advanced uracil-excision DNA engineering. BMC Biotechnol. **10:** 21.

Nour-Eldin, H.H., Geu-Flores, F., and Halkier, B.A. (2010). USER cloning and USER fusion: The ideal cloning techniques for small and big laboratories. In Plant Secondary Metabolism Engineering, A.G. Fett-Neto, ed (New York: Springer), pp. 185–200.

Peiter, E., Maathuis, F.J.M., Mills, L.N., Knight, H., Pelloux, J., Hetherington, A.M., and Sanders, D. (2005). The vacuolar Ca^{2+}-activated channel TPC1 regulates germination and stomatal movement. Nature **434:** 404–408.

Pottosin, I.I., Martínez-Estévez, M., Dobrovinskaya, O.R., Muñiz, J., and Schönknecht, G. (2004). Mechanism of luminal Ca^{2+} and Mg^{2+} action on the vacuolar slowly activating channels. Planta **219:** 1057–1070.

Pottosin, I.I., and Schönknecht, G. (2007). Vacuolar calcium channels. J. Exp. Bot. **58:** 1559–1569.

Ranf, S., Wünnenberg, P., Lee, J., Becker, D., Dunkel, M., Hedrich, R., Scheel, D., and Dietrich, P. (2008). Loss of the vacuolar cation channel, AtTPC1, does not impair Ca^{2+} signals induced by abiotic and biotic stresses. Plant J. **53:** 287–299.

Rienmüller, F., Beyhl, D., Lautner, S., Fromm, J., Al-Rasheid, K.A.S., Ache, P., Farmer, E.E., Marten, I., and Hedrich, R. (2010). Guard cell-specific calcium sensitivity of high density and activity SV/TPC1 channels. Plant Cell Physiol. **51:** 1548–1554.

Robertson, I.M., Sun, Y.B., Li, M.X., and Sykes, B.D. (2010). A structural and functional perspective into the mechanism of Ca^{2+}-sensitizers that target the cardiac troponin complex. J. Mol. Cell. Cardiol. **49:** 1031–1041.

Schönknecht, G., Spoormaker, P., Steinmeyer, R., Brüggeman, L., Ache, P., Dutta, R., Reintanz, B., Godde, M., Hedrich, R., and Palme, K. (2001). KCO1 is a component of the slow-vacuolar (SV) ion channel. FEBS Lett. **511:** 28–32.

Schroeder, J.I., Allen, G.J., Hugouvieux, V., Kwak, J.M., and Waner, D. (2001). Guard cell signal transduction. Annu. Rev. Plant Physiol. Plant Mol. Biol. **52:** 627–658.

Schulze, C., Sticht, H., Meyerhoff, P., and Dietrich, P. (July 7, 2011). Differential contribution of EF-hands to the Ca2+-dependent activation in the plant two-pore channel TPC1. Plant J. http://dx.doi.org/10.1111/j.1365-313X.2011.04697.x

Shaul, O. (2002). Magnesium transport and function in plants: the tip of the iceberg. Biometals **15:** 309–323.

Sheen, J. (2002). A transient expression assay using Arabidopsis mesophyll protoplasts. http://genetics.mgh.harvard.edu/sheenweb/protocols/AtprotoRL04.pdf. Accessed July 12, 2011.

Stühmer, W., Methfessel, C., Sakmann, B., Noda, M., and Numa, S. (1987). Patch clamp characterization of sodium channels expressed from rat brain cDNA. Eur. Biophys. J. **14:** 131–138.

Taiz, L. (1992). The plant vacuole. J. Exp. Biol. **172:** 113–122.

Tufty, R.M., and Kretsinger, R.H. (1975). Troponin and parvalbumin calcium binding regions predicted in myosin light chain and T4 lysozyme. Science **187:** 167–169.

Weinl, S., Held, K., Schlücking, K., Steinhorst, L., Kuhlgert, S., Hippler, M., and Kudla, J. (2008). A plastid protein crucial for Ca^{2+}-regulated stomatal responses. New Phytol. **179:** 675–686.

Yoo, S.D., Cho, Y.H., and Sheen, J. (2007). Arabidopsis mesophyll protoplasts: A versatile cell system for transient gene expression analysis. Nat. Protoc. **2:** 1565–1572.